Correcting charged supercell defect calculations in low-dimensional semiconductors

Chen Zhang,[1] Lei Yan,[2] Chen Qiu,[3] Cai-Xin Zhang,[1] Tao Shen,[1] Su-Huai Wei,[3] and Hui-Xiong Deng[1,*]

[1] *State Key Laboratory of Superlattices and Microstructures, Institute of Semiconductors, Chinese Academy of Sciences, Beijing 100083, China and Center of Materials Science and Optoelectronics Engineering, University of Chinese Academy of Sciences, Beijing 100049, China*

[2] *Science and Technology on Low-Light-Level Night Vision Laboratory, Xi'an 710065, China*

[3] *Beijing Computational Science Research Center, Beijing 100193, China*

(Received 8 October 2023; revised 1 December 2023; accepted 12 December 2023; published 27 December 2023)

Accurate predictions of the nature of defects in low-dimensional materials are essential to enable and promote their applications in micro- and optoelectronic devices. However, when dealing with charged defects in low-dimensional semiconductors, conventional first-principles calculations based on the jellium model encounter the divergence problem, where the formation energy diverges with the vacuum layer thickness. Two promising approaches, the supercell extrapolation method based on the jellium model [Wang *et al.*, Phys. Rev. Lett. **114**, 196801 (2015)] and the real charge model [Xiao *et al.*, Phys. Rev. B **101**, 165306 (2020)], have been proposed to address this divergence issue. However, these two models disagree when extrapolated to an infinitely large supercell following the first-order Makov-Payne correction. Whether they are unified or physically different remains unknown. In this work, we analyze the scaling behaviors of charged defect formation energy in these two computational models. We find that when considering the real charge distribution of ionized charge in two-dimensional systems, an extra quadratic finite-size correction L_S^{-2} (L_S is the lateral supercell size) is required for the formation energy calculations. After this correction, the results of these two models can be unified when extrapolated to infinity following the derived scaling behaviors. Meanwhile, based on the understanding of the differences between these two models, we propose a simple and convenient approach to correct the jellium model error for charged defect calculations in low-dimensional semiconductors. Our work thus provides a practical understanding of the charged defect calculations in low-dimensional semiconductors.

DOI: 10.1103/PhysRevB.108.245305

I. INTRODUCTION

Low-dimensional semiconductors, including transition metal dichalcogenides [1–3], phosphorene [4,5], boron nitride [6,7], quantum dots [8], and more, have received considerable attention for their potential to advance the miniaturization of microelectronic devices and sustain Moore's law. It is widely recognized that defects play a crucial role in determining the properties of low-dimensional semiconductors, serving as the basis for their various functionalities in applications [9–12]. Therefore, the development of our understandings and accurate predictions as well as the engineering of defect properties in low-dimensional semiconductors are of utmost importance.

The first-principles electronic structure calculations based on the density functional theory (DFT) have made significant advances in predicting defect properties of conventional bulk semiconductors [13–15]. Usually, in standard first-principles defect calculations, a finite-size supercell with an embedded defect is used under the periodic boundary condition [15,16]. In this approach, for the charged defects, a jellium model in which uniform background charge is introduced to maintain system neutrality and prevent total energy divergence is often used. However, under this jellium model, the calculated formation energies suffer from slow convergence with respect to the supercell size due to artificial long-range Coulomb interactions between the periodic image charges [15–17], thus finite-size corrections are needed to estimate this error.

In three-dimensional (3D) bulk semiconductors, the Makov-Payne (MP) correction, which scales as $E^{\mathrm{MP}} = a_1 L^{-1} + a_3 L^{-3}$, with $L = \sqrt[3]{V}$ (V being the supercell volume), is often used to correct this image interaction error [16–19]. A modified version of the MP correction was developed by Lany *et al.*, providing consistent schemes to determine the defect quadrupole moment Q and potential alignment [20]. Apart from supercell scaling, Freysoldt *et al.* shows how this supercell artifact can be removed by directly calculating the corresponding electrostatic energy, i.e., Freysoldt-Neugebauer-Van de Walle (FNV) correction [21,22]. Furthermore, alternative approaches involve self-consistently correcting the electrostatic potential (SCPC) to that of the isolate defect charge [23–25], but concerns were raised about the potential neglect of the polarization outside the supercell [21].

For charged defect calculations in low-dimensional semiconductors, the finite-size supercell corrections are more complicated and present significant challenges. Methods that

*Corresponding author: hxdeng@semi.ac.cn

 ©2023 American Physical Society

are practical in 3D cases become limited in low-dimensional systems. Supercell scaling based on the MP correction remains viable [26,27], but the need to include the vacuum layer often results in large supercell sizes, making such calculations expensive [28]. On the other hand, approaches such as the FNV or SCPC correction face limitations, as the dielectric constant profile is required [25–27]. Furthermore, defect calculations in low-dimensional systems typically take the limit $L_z \to \infty$ (L_z being the vacuum layer thickness). However, continuously increasing L_z results in a divergent Coulomb energy. Consequently, the formation energy of the charged defect in the finite-size supercell unrealistically diverges as L_z grows [28]. For this reason, many previous studies have reported widely scattered results with arbitrarily chosen L_z [29–32].

Over the years, some models have been proposed to address this divergence issue, with two categories receiving more attention for their simplicity and practicality. The first type employs a variant of the MP correction, where both the size and shape of the supercell are studied for supercell scaling [28,33–35]. For example, in Ref. [28], Wang *et al.*, based on the jellium model, derived a supercell size dependent analytical formula. Using this formula, they extrapolate the calculated formation energy to $L_z = 0$ to remove the L_z dependent divergence term. It is then found that the extrapolated formation energy linearly scales with the inverse lateral supercell size $L_S^{-1} = \frac{1}{\sqrt{S}}$, where $S = L_x L_y$ is the lateral area of supercell (denoted as the supercell extrapolation method based jellium model or SEJM for convenience). The second type confines the neutralizing charge within a specific region by placing it into artificial or realistic states [36–38]. For example, in the work of Xiao *et al.* [38], they proposed to replace the compensating jellium charge with the real host-band-edge charge (denoted as the transfer to real state model or TRSM for convenience) that is confined within the host structure and can also effectively eliminate the divergence term with L_z. However, results from these two models exhibit a discrepancy when extrapolated to an infinitely large supercell following the first-order MP correction. For example, extrapolated formation energy of charged defects in BN monolayer based on the first-order MP correction shows a discrepancy of 0.14–0.18 eV between these two methods (Fig. 2). This obviously goes against the physical intuition that the results should be consistent as the supercell size tends to infinity. This disparity raises uncertainty about whether these two methods are unified or physically different. Therefore, it is of vital importance to address the physical origin of this discrepancy of these two methods and deepen our understanding for accurate charged defect calculations in low-dimensional semiconductors.

In this paper, we revisit charged defect calculations in low-dimensional semiconductors. In the case of a two-dimensional (2D) system, we analyze the scaling behaviors of the charged defect formation energy under the SEJM and TRSM models. We find that when considering the real charge distribution of the ionized charge in two-dimensional systems, an additional L_S^{-2} correction term is required for the finite-size supercell correction. After this correction, these two models can be effectively unified, as the results obtained from both methods are consistent by the extrapolation to an infinite-size supercell. Furthermore, based on the understanding of the discrepancies between these two models, we also propose a simple and convenient approach to correct the jellium model error for the charged defect calculations in low-dimensional semiconductors, which yields almost the same accuracy as the well-established TRSM methods.

II. METHODS

The formation energy for a charged defect α in its charge state of q is given by [15]

$$\Delta H_f(\alpha, q) = E_{\text{tot}}^{N-q}(\alpha, q) - E_{\text{tot}}^{N_0}(\text{host}) + \sum_i n_i(E_i + \mu_i) + q(E_F + \varepsilon_{\text{VBM}}). \tag{1}$$

$E_{\text{tot}}^{N_0}(\text{host})$ is the total energy of the N_0-electron defect-free host supercell. The integer n_i indicates the number of atoms of type i that have been removed from ($n_i > 0$) or added to ($n_i < 0$) the supercell to form the defect. μ_i is the atomic chemical potential referenced to atomic energy E_i in its stable solid or gas phase. E_{F} is the Fermi energy referenced to the valence band maximum (VBM) ε_{VBM} of the defect-free host system with the same dimensional structure. $E_{\text{tot}}^{N-q}(\alpha, q)$ is the total energy of the defect supercell, where $|q|$ electrons (holes) are removed from the defect state and become ionized charges. As a result, the supercell is left with $N - q$ electrons (N being the electron count of the defect supercell for a neutral defect). To keep the defect supercell charge neutral, a compensating background charge is needed. Usually, the current treatment of this compensating background charge involves two models: the artificial uniform jellium charge [Fig. 1(a), denoted as 3DJM], and the real band-edge charge [Fig. 1(c), denoted as TRSM] [38]. For both treatments, the $E_{\text{tot}}^{N-q}(\alpha, q)$ could suffer from the errors induced by the artificial interaction between the defect charge and its periodic images, as well as the defect charge and compensating background charge for the finite-size supercell calculations. Especially in low-dimensional semiconductors, where dielectric screening is reduced due to the absence of charges in the vacuum layer [27], these artificial interactions are more significant and lead to even larger errors [39]. It is therefore important to identify the errors caused by the two models and the corresponding corrections for the finite-size-supercell defect calculations. Detailed *ab initio* parameter settings for all the data provided can be found in Appendix A.

III. JELLIUM MODEL

First, we revisit charged defect calculations in the 3D jellium model. Actually, the error in the 3DJM-based formation energy $\Delta H_f(\alpha, q, \text{3DJM})$ could be accessed by using a two-dimensional jellium model (2DJM). For the 2DJM, a 2D jellium charge that is uniformly distributed within the material plane is employed for the treatment of the ionized charge [Fig. 1(b)]. In the 2DJM, the ionized charge is confined within the 2D sheet; it can effectively screen the artificial interaction between the defect charge and its image charges across the vacuum region (along the z direction). Consequently, the 2DJM-based total energy of charged defect supercell $E_{\text{tot}}^{N-q}(\alpha, q, \text{2DJM})$ will not diverge with the vacuum layer

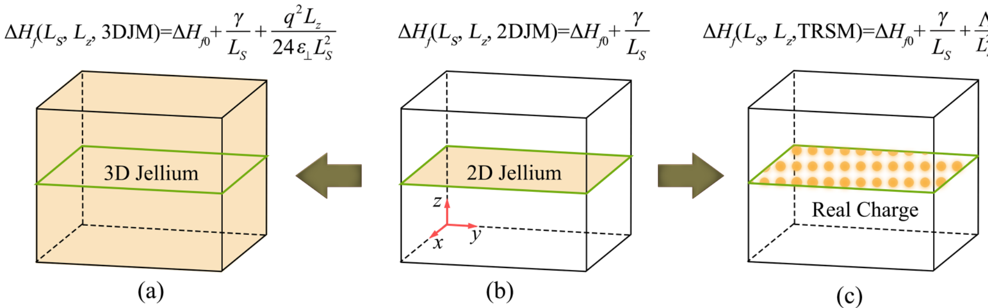

FIG. 1. Charge distribution of the compensating charge in different models: (a) 3D jellium scenario where the ionized charge is distributed uniformly over the whole supercell; (b) 2D jellium scenario where the ionized charge is distributed uniformly within the 2D sheet; (c) real charge scenario where the ionized charge occupies the host-band-edge state with real 2D charge distributions.

thickness L_z. However, the artificial interaction between the defect charge and its image charges within the same layer (i.e., xy plane) still persists. Therefore, considering the dominant periodic defect charge interaction in the 2D xy plane, i.e., 2D Madelung energy $\frac{\gamma}{L_S}$ [40] (γ is the Madelung constant, similar to MP corrections in 3D cases), the total energy of a finite-size charged defect supercell under the 2DJM can be corrected as $E_{\text{tot}}^{N-q}(\alpha,\ q,\ L_S,\ L_z,\ \text{2DJM}) = \text{E}_0^{N-q}(\alpha,\ q,\ L_S,\ L_z) + \frac{\gamma}{L_S}$, where $E_0^{N-q}(\alpha,\ q,\ L_S,\ L_z)$ is the true total energy of the charged defect supercell that is free from any artificial interaction. Thus, based on Eq. (1), the scaling behavior of the charged defect formation energy under the 2DJM is expressed as

$$\Delta H_f(\alpha, q, L_S, L_z, \text{2DJM}) = \Delta H_{f0}(\alpha, q) + \frac{\gamma}{L_S}. \quad (2)$$

Here, $\Delta H_{f0}(\alpha,q)$ denotes the desired true and size-independent formation energy in an infinitely large supercell.

Furthermore, when the compensating charge varies from the 2D jellium charge in the 2DJM [Fig. 1(b)] to the 3D jellium charge in the 3DJM [Fig. 1(a)], the change in electrostatic potential can be expressed as

$$\Delta U_1(\boldsymbol{r}) = \frac{1}{8\pi\varepsilon_\perp}\int d\boldsymbol{r}' \frac{\rho_{\text{3DJM}}(\boldsymbol{r}') - \rho_{\text{2DJM}}(\boldsymbol{r}')}{|\boldsymbol{r}-\boldsymbol{r}'|} = \frac{qL_z}{24\varepsilon_\perp L_S^2}, \quad (3)$$

where $\varepsilon_\perp$ is the dielectric tensor in the z direction, and can be directly calculated by the density functional perturbation theory (DFPT) [41] or the linear response method [42]. The detailed derivation of Eq. (3) can be found in Appendix B. Thus, the total energy of the finite-size charged defect supercell under the 3DJM is given by $E_{\text{tot}}^{N-q}(\alpha,\ q,\ L_S,\ L_z,\ \text{3DJM}) = E_{\text{tot}}^{N-q}(\alpha,\ q,\ L_S,\ L_z,\ \text{2DJM}) + \frac{q^2L_z}{24\varepsilon_\perp L_S^2}$. The scaling behavior of the charged defect formation energy under the conventional 3DJM can then be expressed as

$$\begin{aligned}\Delta H_f&(\alpha, q, L_S, L_z, \text{3DJM}) \\ &= \Delta H_f(\alpha, q, L_S, L_z, \text{2DJM}) + \frac{q^2L_z}{24\varepsilon_\perp L_S^2} \\ &= \Delta H_{\text{f0}}(\alpha, q) + \frac{\gamma}{L_S} + \frac{q^2L_z}{24\varepsilon_\perp L_S^2}. \quad (4)\end{aligned}$$

As expected, the formation energy in the 3DJM linearly diverges as the vacuum layer thickness L_z grows when the L_S is fixed, and Eq. (4) is fully consistent with the findings in Ref. [28], where the derivation has invoked complicated expansions of the formation energy under special cell sizes. We note that for acceptors, this linear dependence fails for large L_z. This is because at large L_z the vacuum level is lowered relative to the defect level by the artificial jellium. The defect charge ends up occupying the unrealistic vacuum state, leading to unreliable results [28]. Moreover, Eq. (4) is also valid for 3D bulk semiconductors, only that $\varepsilon_\perp$ is increased due to better screening for the 3D bulk system. Regardless of the dimensionality of the host semiconductor, supercell scaling can be performed simultaneously in all three directions to fit Eq. (4). We set $L_S = L_z = L = \sqrt[3]{V}$; the extrapolation formula becomes $\Delta H_\text{f}(\alpha,\ q,\ L_S,\ L_z,\ \text{3DJM}) = \Delta H_{f0}(\alpha,\ q) + \frac{\lambda}{L}$, with $\lambda = \gamma + \frac{q^2}{24\varepsilon_\perp}$ and λ being the fitting parameter. Consequently, the extrapolation correction adopts a conventional first-order MP correction. Alternatively, one can first fix the lateral supercell size L_S and extrapolate L_z to $L_z = 0$ to eliminate the L_z linear term in Eq. (4). Then the $L_z = 0$ results can be extrapolated with respect to $\frac{1}{L_S}$ to obtain the desired formation energy in an infinitely large supercell, as demonstrated by Wang *et al.* in Ref. [28], i.e., the SEJM method.

IV. TRSM METHOD

In the following, we can begin our understanding of the TRSM method by comparing it to the 2DJM. Under the TRSM scheme, the ionized charge has a realistic undulating charge distribution constrained within the 2D sheet [Fig. 1(c)], denoted as $\rho_{\text{C,V}}(\boldsymbol{r}) = -q|\psi_{\text{C,V}}(\boldsymbol{r})|^2$, where $\psi_{\text{C,V}}$ is the wave function of the host CBM (VBM) state (CBM is the conduction band minimum). When the charge distribution of the compensating charge shifts from the in-plane jellium charge in the 2DJM [Fig. 1(b)] to the real host-band-edge charge [Fig. 1(c)], the change in the electrostatic potential can be expressed by the difference between the 2D jellium charge and the real charge distributions:

$$\Delta U_2(\boldsymbol{r}) = \frac{1}{8\pi\varepsilon_\parallel}\int d\boldsymbol{r}' \frac{\rho_{\text{C,V}}(\boldsymbol{r}') - \rho_{\text{2DJM}}(\boldsymbol{r}')}{|\boldsymbol{r}-\boldsymbol{r}'|} = \frac{k(\rho_{\text{C,V}},\varepsilon_\parallel)}{S}, \quad (5)$$

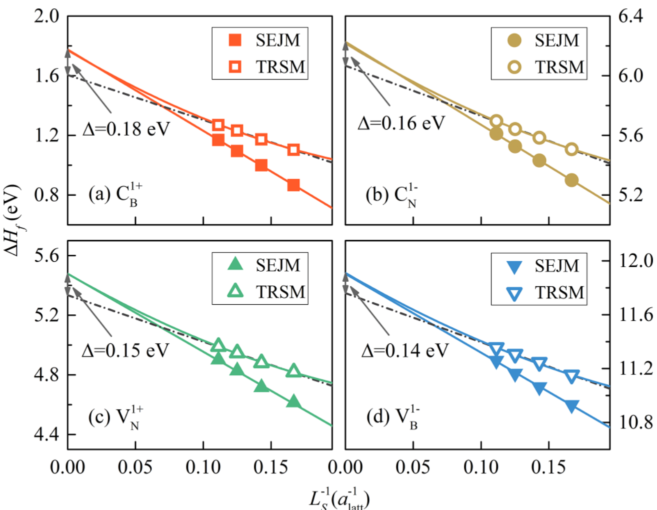

FIG. 2. The extrapolation of the formation energy of (a) C_B^{1+}, (b) C_N^{1-}, (c) V_N^{1+}, and (d) V_B^{1-} in BN monolayer using the SEJM and TRSM methods respectively. a_{latt} is the lateral supercell size in the unit of lattice parameters. The grey dashed lines denote the first-order MP L_S^{-1} extrapolations of the TRSM results. Among all those calculations, the chemical potentials of all elements are set to zero and the Fermi levels are all set to VBM.

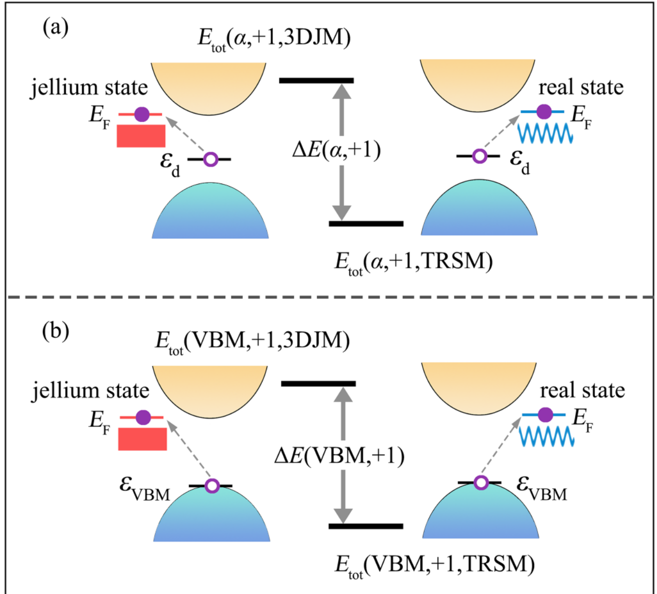

FIG. 3. The schematics of the calculated formation energy of (a) a $q = +1$ donor defect and (b) the $q = +1$ VBM state with 3DJM and TRSM models.

where $k(\rho_{\text{C,V}}, \varepsilon_\parallel)$ is the fitting parameter that depends on the real host-band-edge charge distribution $\rho_{\text{C,V}}(\text{r})$ and the in-plane dielectric constant $\varepsilon_\parallel$. Since it always fulfills that $\int_{\mathbf{r}'\in\text{plane}} d\mathbf{r}' \rho_{\text{2DJM}}(\mathbf{r}') = \int_{\mathbf{r}'\in\text{plane}} d\mathbf{r}' \rho_{\text{C,V}}(\mathbf{r}') = -q$, thus $\rho_{\text{2DJM}}(\mathbf{r}'), \rho_{\text{C,V}}(\mathbf{r}') \propto \frac{1}{S}$, the $\Delta U_2(\mathbf{r})$ term is proportional to $\frac{1}{S}$. Therefore, the total energy of the defect supercell in TRSM should have $E_{\text{tot}}^{N-q}(\alpha,\, q,\, L_S,\, L_z,\, \text{TRSM}) = E_{\text{tot}}^{N-q}(\alpha,\, q,\, L_S,\, L_z,\, \text{2DJM}) + \frac{\Lambda(\rho_{\text{C,V}},\, \varepsilon_\parallel)}{S}$, $\Lambda(\rho_{\text{C,V}}, \varepsilon_\parallel) = qk(\rho_{\text{C,V}}, \varepsilon_\parallel)$ is the fitting parameter and depends on the real charge distributions, and is independent of L_z. Thus, the scaling behavior of the formation energy under TRSM can be written as

$$\Delta H_f(\alpha, q, L_S, L_z, \text{TRSM}) = \Delta H_{f0}(\alpha, q) + \frac{\gamma}{L_S} + \frac{\Lambda(\rho_{\text{C,V}}, \varepsilon_\parallel)}{L_S^2}. \tag{6}$$

In TRSM, the ionized charge naturally occupies the real host-band-edge state, and is constrained within the 2D xy plane. As a result, the artificial interaction between the defect charge and its image charges in the z direction is effectively screened, and the divergent $\frac{q^2 L_z}{24\varepsilon_\perp L_S^2}$ term is no longer presented. Thus, the charged defect formation energy from the TRSM method remains convergent as the vacuum layer thickness grows when the lateral supercell size S is fixed, consistent with Ref. [38]. Furthermore, for asymptotic extrapolation based on the TRSM, the finite-size correction of the charge defect formation energy requires an additional quadratic L_S^{-2} term. This extra L_S^{-2} term accounts for the electrostatic difference between 2D undulating charge and in-plane jellium charge. It is therefore needed not only for the TRSM, but also for other models using the 2D undulating charge as the compensating charge [36,37]. To address the consistency of the TRSM method with the SEJM method, Fig. 2 displays the extrapolation of the formation energy of C_B^{1+}, C_N^{1-}, V_N^{1+}, and V_B^{1-} in BN monolayer derived from both methods. Within the L_S^{-2} correction fitting in the TRSM method, the extrapolated formation energies from both methods are identical (with an error less than 0.01 eV), indicating that both calculation schemes are equivalent and can be effectively unified. Note that the TRSM method is more straightforward and physically intuitive, making it more suitable for practical applications in low-dimensional materials.

V. AN ALTERNATIVE CORRECTION SCHEME

Now that we have figured out the origin of the difference between the TRSM model and the JM model, next we can explore how to correct the charged defect formation energy from the 3DJM to that of the TRSM. To facilitate the discussion, we consider a $q = +1$ donor as an example. Combining Eqs. (4) and (6), the difference in TRSM-based and 3DJM-based charged defect formation energy [$\Delta E(\alpha, +1)$, Fig. 3(a)] is

$$\begin{aligned}\Delta E(\alpha, +1) &= \Delta H_f(\alpha, +1, \text{TRSM}) - \Delta H_f(\alpha, +1, \text{3DJM})\\ &= \frac{\Lambda(\rho_{\text{C,V}}, \varepsilon_\parallel)}{L_S^2} - \frac{L_z}{24\varepsilon_\perp L_S^2}.\end{aligned} \tag{7}$$

Directly calculating Eq. (7) is challenging due to the unknown fitting parameter Λ and the difficulty in defining $\varepsilon_\perp$. Nonetheless, we note that $\Delta E(\alpha, +1)$ mainly depends on the supercell size (L_S, L_z), the dielectric tensor of the host material ($\varepsilon_\parallel$, $\varepsilon_\perp$), and the charge distribution of the band-edge state $\rho_{\text{C,V}}$. Thus, these quantities are mainly the host system properties. This is expected since the TRSM method and the 3DJM only differ in their treatments of the ionized charge [Fig. 3(a)]. Technically we could reproduce this difference by calculations solely with the host structure. In this case, we can

consider the VBM state as a special donor state, and when an electron is excited from the VBM to jellium E_F state in the 3DJM, it may produce the same error as that excited from the defect state. The difference in formation energies for the VBM as a donor defect state between the TRSM and 3DJM models is $\Delta E(\text{VBM}, +1) = \Delta H_f(\text{VBM}, +1, \text{TRSM}) - \Delta H_f(\text{VBM}, +1, \text{3DJM})$ [Fig. 3(b)]. Similar to the $\Delta E(\alpha, +1)$, $\Delta E(\text{VBM}, +1)$ is also determined by the difference in the charge distribution between the 3D jellium charge and the real charge [Fig. 3(b)]. Thus, under the same supercell size $\Delta E(\text{VBM}, +1)$ could be almost equal to $\Delta E(\alpha, +1)$. It should be noted that although the charge distribution between the donor defect (ρ_d) and VBM state (ρ_{VBM}) is different, as both the donor defect charge and the VBM charge are localized in the z direction, this difference tends to be small. A similar discussion also holds for acceptors.

Therefore, we propose an alternative simple and convenient method for the jellium charge corrections (JCCs), under which the charged defect formation energy can be corrected by

$$\Delta H_f(\alpha, q, \text{JCC}) = \Delta H_f(\alpha, q, \text{3DJM}) + \delta E_0, \quad (8)$$

where $\delta E_0 = E_{\text{tot}}^{N_0}(\text{host}, L_S, L_z) - E_{\text{tot}}^{N_0-q}(\text{host}, q, L_S, L_z, \text{3DJM}) - q\varepsilon_b$, $\varepsilon_b = \varepsilon_{\text{VBM}}$ for $q > 0$ and $\varepsilon_b = \varepsilon_{\text{CBM}}$ for $q < 0$ can be calculated from the host system to simulate ΔE. The JCC correction cancels out errors arising from treating the ionized charge as the artificial jellium charge in the 3DJM model, and $\Delta H_f(\alpha, q, \text{JCC})$ is expected to obtain a reliable accurate formation energy comparable to that from the TRSM method for the finite-size-supercell calculations. We note that this JCC correction method can be applicable to semiconductors of arbitrary dimensionality. In conventional 3D semiconductors, due to the large dielectric screening and the small difference in charge distribution between the host-band-edge charge and the 3D jellium charge (since both of them are fully delocalized in the whole supercell), the correction term δE_0 is small and can be ignored [38,43] (see Fig. 5 in Appendix C). Thus, the conventional 3DJM usually yields accurate formation energies for charged defects in 3D bulk semiconductors. However, in low-dimensional semiconductors, because the host-band-edge charge is no longer distributed in the whole supercell, a large disparity arises in the charge distribution between the host-band-edge charge and the 3D jellium charge. The 3D jellium charge can no longer serve as a reliable approximation for the host-band-edge charge. δE_0 is now no longer small and should be taken into serious consideration [38] (see Fig.5 in Appendix C).

To prove the applicability of the JCC method, we show in Fig. 4(a) the comparison between formation energies calculated with the JCC scheme and the TRSM scheme for different point defects in various low-dimensional materials, such as WSe_2 monolayer, GeS monolayer, black phosphorene, black arsenene, BN monolayer and (3, 3) BN nanotube. It can clearly be seen that the JCC corrected results have reached excellent agreement with those derived by the TRSM. The root mean square error of all considered defects is only about a dozen meV (see Table I in Appendix D). The success of the JCC method in (3, 3) BN nanotube has also proved its applicability in 1D systems. Obviously, with this correction, it is

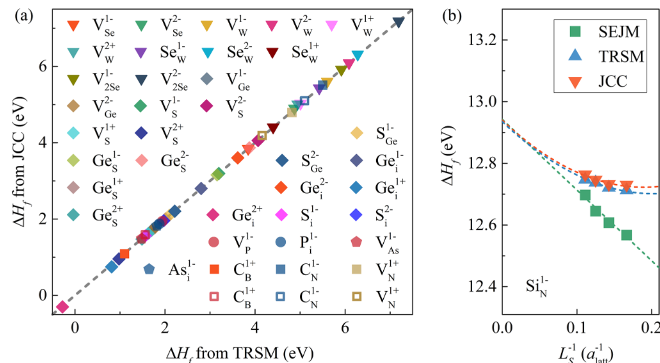

FIG. 4. (a) Comparison of formation energies of charged point defects in WSe_2 monolayer ($L_z = 30$ Å, 6×6, inverted triangles), GeS monolayer ($L_z = 20$ Å, 6×6, diamonds), black phosphorene ($L_z = 20$ Å, 6×6, round dots), black arsenene ($L_z = 20$ Å, 6×6, pentagons), BN monolayer ($L_z = 30$ Å, 6×6, solid squares) and (3, 3) BN nanotube ($L_x = L_y = 25$ Å, $a_{\text{latt}} = 9$, hollow squares) calculated by the JCC and TRSM methods. (b) The extrapolation of formation energy of Si_N^{1-} in BN monolayer to infinity using the SEJM, TRSM, and JCC schemes respectively. Among all calculations, the chemical potentials of all elements are set to zero and the Fermi levels are all set to VBM.

also easy to obtain $\Delta H_{f0}(\alpha,q)$ by extrapolating L_S to infinity. As shown in Fig. 4(b), the TRSM, JCC, and SEJM apparently have the same $\Delta H_{f0}(\alpha,q)$ in the case of infinite supercell size. Compared to the SEJM method, the JCC method stands out for its simplicity, as it eliminates the linear extrapolation with L_z. Furthermore, it has a much wider range of applications, since its applications are not limited to 2D systems, but can also be applied to other low-dimensional systems, such as nanotubes, quantum dots, etc.

VI. CONCLUSIONS

In conclusion, we have addressed the previously observed discrepancy between the SEJM and TRSM methods. Despite these two methods differing in the treatment of the ionized charge, based on the first-order MP correction, they can be unified when extrapolated to infinity even though they have the different extrapolation formulas. Furthermore, we proposed a simple and convenient JCC method for the finite-size-supercell corrections of the charged defect calculations in low-dimensional semiconductors. The JCC correction cancels out errors arising from treating the ionized charge as the artificial jellium charge in the 3DJM model and exhibits the same accuracy with the TRSM results. Our work has thus provided a practical understanding of charged defect calculations in low-dimensional semiconductors.

ACKNOWLEDGMENTS

This work was supported by the National Natural Science Foundation of China (Grants No. 12174099, No. 61922077, No. 11874347, No. 12088101, No. 11991060, and No. U2230402), the National Key Research and Development Program of China (Grants No. 2018YFB2200100 and No.

2020YFB1506400), the Key Research Program of the Chinese Academy of Sciences (Grant No. XDB0460000), and the CAS Project for Young Scientists in Basic Research (Grant No. YSBR-026). H.-X.D. was also supported by the Youth Innovation Promotion Association of Chinese Academy of Sciences (Grant No. Y2021042).

APPENDIX A: COMPUTATIONAL DETAILS

Our DFT calculations were performed using QUANTUM ESPRESSO *ab initio* codes [44,45]. The Perdew-Burke-Ernzerhof functional [46] was selected as the exchange and correlation potential. The valence electrons are described by the norm-conserving pseudopotentials [47,48]. The kinetic energy cutoff was set to 70 Ry, and the energy convergence threshold was set to 10^{-12} Ry. A Γ-centered k-point mesh with $2\pi \times 0.03$ Å^{-1} spacing was used for primitive cell calculations, and a single k-point grid was employed for defect supercell calculations. All atoms were fully relaxed until the Hellmann-Feynman force on each atom reaches less than 10^{-8} Ry/Bohr.

APPENDIX B: SCALING BEHAVIOR OF $\Delta U_1(\boldsymbol{R})$

In Eq. (3) in the main text, the $\Delta U_1(\boldsymbol{r})$ term originates from charge distribution difference of the ionized carriers between 3DJM and 2DJM. In the host structure, we can expand the periodically distributed charge with the reciprocal vectors:

$$\rho(\boldsymbol{r}) = \sum_{\mathbf{G}} \rho(\mathbf{G}) e^{i\mathbf{G}\cdot\boldsymbol{r}}, \tag{B1}$$

$$\rho(\mathbf{G}) = \frac{1}{V_0} \int_{\boldsymbol{r}\in pc} d\boldsymbol{r}\, \rho(\boldsymbol{r}) e^{-i\mathbf{G}\cdot\boldsymbol{r}}, \tag{B2}$$

in which V_0 is the volume of primitive cell with lattice parameters of $a \times a \times L_z$; we assume that N_{pc} primitive cells are included in our deductions. The integral $\int_{\boldsymbol{r}\in pc} d\boldsymbol{r}$ is done within the primitive cell. For convenience we denote the charge distribution's Fourier component corresponded to reciprocal wave vector $G(m, n, p) = m\frac{2\pi}{a}\vec{x} + n\frac{2\pi}{a}\vec{y} + p\frac{2\pi}{L_z}\vec{z}$ as $\rho(m, n, p)$; then it is evident that $\rho(m, n, p) \neq 0$ only when $m = n = p = 0$ for the 3DJM and only when $m = n = 0$ for the 2DJM. Furthermore, for a charged defect (α, q), we have $\rho_{3DJM}(0, 0, 0) = \rho_{2DJM}(0, 0, p) = \frac{-q}{SL_z}$, where $S = L_x L_y$ is the lateral area of the supercell. We have

$$\Delta U_1(\boldsymbol{r}) = \frac{1}{8\pi\varepsilon_0} \int d\boldsymbol{r}' \frac{\rho_{3DJM}(\boldsymbol{r}') - \rho_{2DJM}(\boldsymbol{r}')}{|\boldsymbol{r} - \boldsymbol{r}'|}$$

$$= -\frac{1}{8\pi\varepsilon_0} \int d\boldsymbol{r}' \frac{1}{N_{pc} V_0} \sum_{k} \frac{4\pi}{\boldsymbol{k}^2} e^{i\boldsymbol{k}\cdot(\boldsymbol{r}-\boldsymbol{r}')} \times \sum_{\mathbf{G}\neq 0} \rho_{2DJM}(\mathbf{G}) e^{i\mathbf{G}\cdot\boldsymbol{r}'}$$

$$= -\frac{1}{2\varepsilon_0} \sum_{\mathbf{G}\neq 0} \frac{\rho_{2DJM}(\mathbf{G})}{\mathbf{G}^2} e^{i\mathbf{G}\cdot\boldsymbol{r}}$$

$$= -\frac{1}{8\pi^2\varepsilon_0} \sum_{m^2+n^2+p^2\neq 0} \frac{\rho_{2DJM}(m, n, p)}{\frac{m^2+n^2}{a^2} + \frac{p^2}{L_z^2}} e^{i\mathbf{G}(m,n,p)\cdot\boldsymbol{r}}$$

$$= -\frac{1}{8\pi^2\varepsilon_0} \sum_{p\neq 0} \frac{\rho_{2DJM}(0, 0, p)}{p^2/L_z^2} e^{i\mathbf{G}(0,0,p)\cdot z}$$

$$= \frac{qL_z}{8\pi^2\varepsilon_0 S} \sum_{p\neq 0} \frac{1}{p^2} = \frac{qL_z}{24\varepsilon_0 S}. \tag{B3}$$

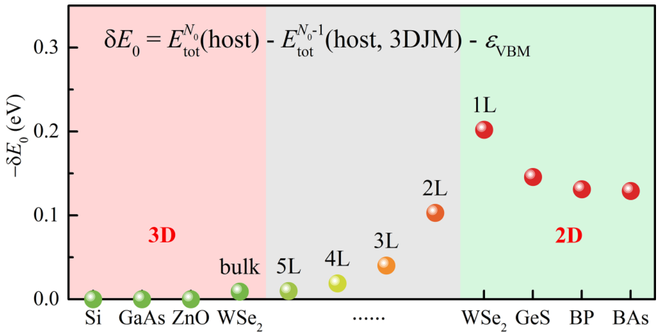

FIG. 5. The JCC correction term (δE_0) in Si ($4 \times 4 \times 4$, 512 atoms), GaAs ($4 \times 4 \times 4$, 512 atoms), ZnO ($4 \times 4 \times 4$, 512 atoms), GeS monolayer ($L_z = 20$ Å, 6×6), black phosphorene ($L_z = 20$ Å, 6×6), black arsenene ($L_z = 20$ Å, 6×6), and WSe_2 ($L_z = 41.45$ Å, 10×10). For WSe_2, the attached labels represent the number of layers in the supercell.

APPENDIX C: COMPARISON OF THE CORRECTION TERM IN 3D AND 2D MATERIALS

In order to compare the correction term in 3D and 2D materials, we calculated the JCC correction term $\delta E_0 = E_{tot}^{N_0}(\text{host}) - [E_{tot}^{N_0-1}(\text{host, 3DJM}) + \varepsilon_{VBM}]$ in Si ($4 \times 4 \times 4$, 512 atoms), GaAs ($4 \times 4 \times 4$, 512 atoms), ZnO ($4 \times 4 \times 4$, 512 atoms), GeS monolayer ($L_z = 20$ Å, 6×6), black phosphorene ($L_z = 20$ Å, 6×6), black arsenene ($L_z = 20$ Å, 6×6), WSe_2 monolayer ($L_z = 41.45$ Å, 10×10). For WSe_2, we begin with the layered bulk structure (with six layers in the supercell, bulk in the 3D region of Fig. 5), and reduce the number of layers (grey region of Fig. 5), until it reaches a monolayer ($1L$ in the 2D region of Fig. 5). As shown in Fig. 5, the JCC correction term in 3D bulk semiconductors (red region) is small and can usually be ignored. However, it gradually increases as the 2D characteristics of the host structure become more prominent (grey region). Ultimately, the JCC correction term becomes very large in 2D systems (green region) and thus cannot be neglected.

APPENDIX D: COMPARISON BETWEEN JCC AND TRSM

To verify the effectiveness of the JCC method more directly, we present in Table I in detail the formation energies of charged defects calculated using the JCC and TRSM method in different two-dimensional materials, including

TABLE I. List of JCC corrected formation energies versus TRSM results for various charged points in different systems.

Systems	Defect	ΔH_f (eV) JCC	ΔH_f (eV) TRSM	Systems	Defect	ΔH_f (eV) JCC	ΔH_f (eV) TRSM
WSe_2 monolayer	V_{Se}^{1-}	3.846	3.847	GeS monolayer	Ge_S^{2+}	1.473	1.489
	V_{Se}^{2-}	4.899	4.875		S_{Ge}^{1-}	2.098	2.099
	V_W^{1-}	5.603	5.602		S_{Ge}^{2-}	2.204	2.216
	V_W^{2-}	6.089	6.086		Ge_i^{1-}	2.801	2.804
	V_W^{1+}	5.024	5.009		Ge_i^{2-}	3.604	3.616
	V_W^{2+}	4.981	4.942		Ge_i^{1+}	0.768	0.815
	Se_W^{1-}	5.430	5.425		Ge_i^{2+}	-0.301	−0.277
	Se_W^{2-}	6.315	6.279		S_i^{1-}	1.563	1.566
	Se_W^{1+}	4.402	4.402		S_i^{2-}	1.959	1.975
	V_{2Se}^{1-}	5.916	5.916	Black phosphorene	V_p^{1-}	1.940	1.937
	V_{2Se}^{2-}	7.183	7.189		p_i^{1-}	1.874	1.872
GeS monolayer	V_{Ge}^{1-}	1.703	1.704	Black arsenene	V_{As}^{1-}	1.485	1.483
	V_{Ge}^{2-}	1.769	1.773		As_i^{1-}	1.825	1.823
	V_S^{1-}	3.194	3.195	BN monolayer	C_B^{1+}	1.089	1.104
	V_S^{2-}	4.057	4.068		C_N^{1-}	5.507	5.504
	V_S^{1+}	1.625	1.630		V_N^{1+}	4.792	4.820
	V_S^{2+}	0.956	0.978	(3, 3) BN nanotube	C_B^{1+}	1.590	1.561
	Ge_S^{1-}	3.155	3.156		C_N^{1-}	5.101	5.098
	Ge_S^{2-}	3.868	3.874		V_N^{1+}	4.187	4.159
	Ge_S^{1+}	2.005	2.010				
Root mean square error (eV)					0.017		

WSe_2 monolayer ($L_z = 30$ Å, 6×6), GeS monolayer ($L_z = 20$ Å, 6×6), black phosphorene ($L_z = 20$ Å, 6×6), black arsenene ($L_z = 20$ Å, 6×6), BN monolayer ($L_z = 30$ Å, 6×6) and (3, 3) BN nanotube ($L_x = L_y = 25$ Å, $a_{\mathrm{latt}} = 9$). The corresponding correction terms are presented in Table II. Among all those calculations, the chemical potentials of all elements are set to zero and Fermi levels are all set to $\varepsilon_{\mathrm{VBM}}$. We can see that the two methods agree in the range of a dozen meV, which directly illustrates the validity of the JCC method.

TABLE II. The JCC correction term δE_0 (eV) in different systems.

Systems	q	δE_0 (eV)	Systems	q	δE_0 (eV)
WSe_2 monolayer ($L_z = 30$ Å, 6×6)	+1	−0.352	Black phosphorene ($L_z = 20$ Å, 6×6)	+1	−0.131
	+2	−1.434		−1	−0.147
	−1	−0.348	Black arsenene ($L_z = 20$ Å, 6×6)	+1	−0.130
	−2	−1.424		−1	−0.129
GeS monolayer ($L_z = 20$ Å, 6×6)	+1	−0.140	BN monolayer ($L_z = 30$ Å, 6×6)	+1	−0.943
	+2	−0.557		−1	−0.943
	−1	−0.140	(3, 3) BN nanotube ($L_x = L_y = 25$ Å, $a_{\mathrm{latt}} = 9$)	+1	−0.434
	−2	−0.557		−1	−0.458

[1] B. Radisavljevic, A. Radenovic, J. Brivio, V. Giacometti, and A. Kis, Single-layer MoS_2 transistors, Nat. Nanotechnol. **6**, 147 (2011).
[2] Q. H. Wang, K. Kalantar-Zadeh, A. Kis, J. N. Coleman, and M. S. Strano, Electronics and optoelectronics of two-dimensional transition metal dichalcogenides, Nat. Nanotechnol. **7**, 699 (2012).
[3] K. F. Mak and J. Shan, Photonics and optoelectronics of 2D semiconductor transition metal dichalcogenides, Nat. Photonics **10**, 216 (2016).
[4] L. Li, Y. Yu, G. J. Ye, Q. Ge, X. Ou, H. Wu, D. Feng, X. H. Chen, and Y. Zhang, Black phosphorus field-effect transistors, Nat. Nanotechnol. **9**, 372 (2014).
[5] E. Samuel Reich, Phosphorene excites materials scientists, Nature (London) **506**, 19 (2014).
[6] D. Pacilé, J. C. Meyer, Ç. Ö. Girit, and A. Zettl, The two-dimensional phase of boron nitride: Few-atomic-layer sheets and suspended membranes, Appl. Phys. Lett. **92**, 133107 (2008).
[7] M. Xu, T. Liang, M. Shi, and H. Chen, Graphene-like two-dimensional materials, Chem. Rev. **113**, 3766 (2013).
[8] M. Liu, N. Yazdani, M. Yarema, M. Jansen, V. Wood, and E. H. Sargent, Colloidal quantum dot electronics, Nat. Electron. **4**, 548 (2021).
[9] A. Ziletti, A. Carvalho, D. K. Campbell, D. F. Coker, and A. H. Castro Neto, Oxygen defects in phosphorene, Phys. Rev. Lett. **114**, 046801 (2015).
[10] Z. Lin, B. R. Carvalho, E. Kahn, R. Lv, R. Rao, H. Terrones, M. A. Pimenta, and M. Terrones, Defect engineering of two-dimensional transition metal dichalcogenides, 2D Mater. **3**, 022002 (2016).
[11] J. Pei, X. Gai, J. Yang, X. Wang, Z. Yu, D. Y. Choi, B. Luther-Davies, and Y. Lu, Producing air-stable monolayers of phosphorene and their defect engineering, Nat. Commun. **7**, 10450 (2016).
[12] J. Hong, C. Jin, J. Yuan, and Z. Zhang, Atomic defects in two-dimensional materials: From single-atom spectroscopy to functionalities in opto-/electronics, nanomagnetism, and catalysis, Adv. Mater. **29**, 1606434 (2017).
[13] S.-H. Wei and S. B. Zhang, Chemical trends of defect formation and doping limit in II-VI semiconductors: The case of CdTe, Phys. Rev. B **66**, 155211 (2002).
[14] S.-H. Wei, Overcoming the doping bottleneck in semiconductors, Comput. Mater. Sci. **30**, 337 (2004).
[15] C. Freysoldt, B. Grabowski, T. Hickel, J. Neugebauer, G. Kresse, A. Janotti, and C. G. Van de Walle, First-principles calculations for point defects in solids, Rev. Mod. Phys. **86**, 253 (2014).
[16] M. Leslie and N. J. Gillan, The energy and elastic dipole tensor of defects in ionic crystals calculated by the supercell method, J. Phys. C: Solid State Phys. **18**, 973 (1985).
[17] G. Makov and M. C. Payne, Periodic boundary conditions in *ab initio* calculations, Phys. Rev. B **51**, 4014 (1995).
[18] C. W. M. Castleton, A. Höglund, and S. Mirbt, Managing the supercell approximation for charged defects in semiconductors: Finite-size scaling, charge correction factors, the band-gap problem, and the *ab initio* dielectric constant, Phys. Rev. B **73**, 035215 (2006).
[19] J. Shim, E.-K. Lee, Y. J. Lee, and R. M. Nieminen, Density-functional calculations of defect formation energies using supercell methods: Defects in diamond, Phys. Rev. B **71**, 035206 (2005).
[20] S. Lany and A. Zunger, Accurate prediction of defect properties in density functional supercell calculations, Modell. Simul. Mater. Sci. Eng. **17**, 084002 (2009).
[21] C. Freysoldt, J. Neugebauer, and C. G. Van de Walle, Fully *ab initio* finite-size corrections for charged-defect supercell calculations, Phys. Rev. Lett. **102**, 016402 (2009).
[22] Y. Kumagai and F. Oba, Electrostatics-based finite-size corrections for first-principles point defect calculations, Phys. Rev. B **89**, 195205 (2014).
[23] P. A. Schultz, Charged local defects in extended systems, Phys. Rev. Lett. **84**, 1942 (2000).
[24] I. Dabo, B. Kozinsky, N. E. Singh-Miller, and N. Marzari, Electrostatics in periodic boundary conditions and real-space corrections, Phys. Rev. B **77**, 115139 (2008).
[25] M. Chagas da Silva, M. Lorke, B. Aradi, M. Farzalipour Tabriz, T. Frauenheim, A. Rubio, D. Rocca, and P. Deák, Self-consistent potential correction for charged periodic systems, Phys. Rev. Lett. **126**, 076401 (2021).
[26] H. P. Komsa and A. Pasquarello, Finite-size supercell correction for charged defects at surfaces and interfaces, Phys. Rev. Lett. **110**, 095505 (2013).
[27] H.-P. Komsa, N. Berseneva, A. V. Krasheninnikov, and R. M. Nieminen, Charged point defects in the flatland: Accurate formation energy calculations in two-dimensional materials, Phys. Rev. X **4**, 031044 (2014).
[28] D. Wang, D. Han, X. B. Li, S. Y. Xie, N. K. Chen, W. Q. Tian, D. West, H. B. Sun, and S. B. Zhang, Determination of formation and ionization energies of charged defects in two-dimensional materials, Phys. Rev. Lett. **114**, 196801 (2015).
[29] B. Huang and H. Lee, Defect and impurity properties of hexagonal boron nitride: A first-principles calculation, Phys. Rev. B **86**, 245406 (2012).
[30] S. Okada, Atomic configurations and energetics of vacancies in hexagonal boron nitride: First-principles total-energy calculations, Phys. Rev. B **80**, 161404(R) (2009).
[31] C. Xia, Y. Peng, S. Wei, and Y. Jia, The feasibility of tunable *p*-type Mg doping in a GaN monolayer nanosheet, Acta Mater. **61**, 7720 (2013).
[32] Y. Peng, C. Xia, H. Zhang, T. Wang, S. Wei, and Y. Jia, Tunable electronic structures of *p*-type Mg doping in AlN nanosheet, J. Appl. Phys. **116**, 044306 (2014).
[33] N. D. M. Hine, K. Frensch, W. M. C. Foulkes, and M. W. Finnis, Supercell size scaling of density functional theory formation energies of charged defects, Phys. Rev. B **79**, 024112 (2009).
[34] S. T. Murphy and N. D. M. Hine, Anisotropic charge screening and supercell size convergence of defect formation energies, Phys. Rev. B **87**, 094111 (2013).
[35] D. Wang, D. Han, X.-B. Li, N.-K. Chen, D. West, V. Meunier, S. Zhang, and H.-B. Sun, Charged defects in two-dimensional semiconductors of arbitrary thickness and geometry: Formulation and application to few-layer black phosphorus, Phys. Rev. B **96**, 155424 (2017).
[36] N. A. Richter, S. Sicolo, S. V. Levchenko, J. Sauer, and M. Scheffler, Concentration of vacancies at metal-oxide surfaces: Case study of MgO(100), Phys. Rev. Lett. **111**, 045502 (2013).

[37] O. Sinai, O. T. Hofmann, P. Rinke, M. Scheffler, G. Heimel, and L. Kronik, Multiscale approach to the electronic structure of doped semiconductor surfaces, Phys. Rev. B **91**, 075311 (2015).

[38] J. Xiao, K. Yang, D. Guo, T. Shen, H.-X. Deng, S.-S. Li, J.-W. Luo, and S.-H. Wei, Realistic dimension-independent approach for charged-defect calculations in semiconductors, Phys. Rev. B **101**, 165306 (2020).

[39] J. Lento, J. L. Mozos, and R. M. Nieminen, Charged point defects in semiconductors and the supercell approximation, J. Phys.: Condens. Matter **14**, 2637 (2002).

[40] P. C. Pereira and S. W. Apolinario, Madelung energy of Yukawa lattices, Phys. Rev. E **86**, 046702 (2012).

[41] X. Wu, D. Vanderbilt, and D. R. Hamann, Systematic treatment of displacements, strains, and electric fields in density-functional perturbation theory, Phys. Rev. B **72**, 035105 (2005).

[42] I. Souza, J. Íñiguez, and D. Vanderbilt, First-principles approach to insulators in finite electric fields, Phys. Rev. Lett. **89**, 117602 (2002).

[43] S. B. Zhang, S.-H. Wei, A. Zunger, and H. Katayama-Yoshida, Defect physics of the $CuInSe_2$ chalcopyrite semiconductor, Phys. Rev. B **57**, 9642 (1998).

[44] P. Giannozzi *et al.*, QUANTUM ESPRESSO: A modular and open-source software project for quantum simulations of materials, J. Phys.: Condens. Matter **21**, 395502 (2009).

[45] P. Giannozzi *et al.*, Advanced capabilities for materials modelling with QUANTUM ESPRESSO, J. Phys.: Condens. Matter **29**, 465901 (2017).

[46] J. P. Perdew, K. Burke, and M. Ernzerhof, Generalized gradient approximation made simple, Phys. Rev. Lett. **77**, 3865 (1996).

[47] P. E. Blochl, Projector augmented-wave method, Phys. Rev. B **50**, 17953 (1994).

[48] G. Kresse and J. Furthmüller, Efficient iterative schemes for ab initio total-energy calculations using a plane-wave basis set, Phys. Rev. B **54**, 11169 (1996).